Available online at www.sciencedirect.com

SciVerse ScienceDirect

Ceramics International 39 (2013) 673–682

CERAMICS INTERNATIONAL

www.elsevier.com/locate/ceramint

Microstructure and mechanical properties of alumina 5 vol% zirconia nanocomposites prepared by powder coating and powder mixing routes

Frank Kern[a], Paola Palmero[b,*]

[a]University of Stuttgart, IFKB, Allmandring 7b, D-70569 Stuttgart, Germany
[b]Department of Applied Science and Technology, INSTM—R.U. PoliTO—LINCE Lab., Politecnico di Torino, Corso Duca degli Abruzzi, 24, 10129 Torino, Italy

Received 3 April 2012; received in revised form 22 May 2012; accepted 26 June 2012
Available online 1 July 2012

Abstract

Zirconia toughened alumina (ZTA) nanocomposites are attractive structural materials which combine the high hardness and Young's modulus of the alumina matrix with an additional toughening effect by the zirconia dispersion.

In this study two approaches to prepare ZTA are compared. For the first approach, an ultrafine alumina powder was coated with 5 vol% zirconia by a wet chemical method. For the second one, the reference material was prepared by intensively mixing and milling the same alumina with nanoscale zirconia powder. Samples were consolidated at 1350–1600 °C by hot pressing and their mechanical properties, microstructure and transformation behavior were compared. Toughness increments derived from different toughening mechanisms are also briefly discussed. Besides better sinterability, the mixed material exhibited a finer grain size of both matrix and dispersion and thus higher hardness and strength. The alumina matrix was under compressive hydrostatic residual cooling stress, whereas zirconia was under tensile one. The coated material, however, showed higher transformability, deeper transformation zones and thus higher fracture toughness. In addition, it contained more monoclinic zirconia so the matrix was under tension.

Keywords: B. Microstructure-final; C. Mechanical properties; D. Al_2O_3; D. ZrO_2

1. Introduction

Zirconia toughened alumina is probably the technically most widely used composite oxide structural ceramic. ZTA materials have been used for decades for wear parts and cutting tools due to their high strength, hardness, toughness and abrasion resistance [1]. In recent years ZTA has become increasingly important as a structural material for biomedical implants with drastically reduced low temperature degradation compared to yttria stabilized zirconia (Y-TZP) [2]. The most important reinforcement mechanisms active in ZTA are transformation toughening and microcracking [3]. Microcracking is favoured in ZTA with large unstabilized zirconia inclusions which become monoclinic during cooling. This leaves a network of microcracks in the alumina matrix which enables high toughness but limits strength [4]. Stress induced martensitic phase transformation occurs in ZTA if the dispersion is kept tetragonal and transformable. This requires the control of stabilizer content and grain size [5]. Faceted inter-granular zirconia grains are more transformable than modular grains incorporated into the alumina matrix. The microstructure plays a key role in the development of high performance ZTA [6]. Recently the role of different dopants on the development of ZTA microstructures have been demonstrated [7]. In the early days of ZTA development, wet chemical methods such as coprecipitation were successfully tried in order to produce highly dispersed powders [8]. Today mixing and milling processes starting from commercially available alumina and zirconia powders are preferred for economic aspects. It was shown however that the coating

*Corresponding author. Tel.: +39 0115644678; fax: +39 0115644699.
E-mail address: paola.palmero@polito.it (P. Palmero).

0272-8842/$36.00
http://dx.doi.org/10.1016/j.ceramint.2012.06.078

of alumina with a zirconia precursor can improve the homogeneity of the zirconia dispersion [9]. Our previous works have dealt with the development of a reproducible coating process and the subsequent heat treatment cycles necessary for dispersing and fixing the zirconia on ultrafine alumina powders. This can avoid coagulation of the zirconia nuclei and improve the homogeneity of the system [10,11]. In a subsequent study, the sintering cycle was modeled in order to optimize final density and microstructural development [12]. In spite of such advances in ZTA processing techniques, our latest results on strong and tough ZTA materials produced from submicron size alumina and nanoscale zirconia powders have demonstrated that the mixing and milling technology is not necessarily inferior if the dispersion quality is high [13,14].

The present study was carried out in order to compare the characteristics of ZTA materials manufactured from two different preparation methods. In the first case, a commercial alumina powder was coated with a zirconia precursor. In the second one, the same alumina was milled with nanosized commercial zirconia powders. The powders were hot-pressed under identical sintering conditions. The mechanical properties could therefore be linked to the microstructural evolution and phase compositions, to gain a deeper understanding on the processes elapsing.

2. Experimental

2.1. Powder processing and sintering

Both feedstocks of Alumina-5vol-% ZrO_2 (AZ5) powder were prepared starting from the same batch of α-alumina (TM-DAR, Taimicron, Japan, $d_{50}=150$ nm, $S_{BET}=14.5\ m^2/g$). The percentage of 5 vol% zirconia was calculated assuming that zirconia is fully tetragonal ($6.05\ g/cm^3$) in the final composites. For the coated ZTA powder, hereafter named as AZ5C, a well dispersed alumina suspension was mixed with an aqueous solution of zirconium chloride. The doped slurry was maintained under magnetic stirring for 2 h and then spray dried. The powder (80 g) was calcined at 600 °C for 1 h, to decompose the synthesis by-products (mainly chlorides) and to induce the crystallization of tetragonal zirconia on the alumina surface [12,15]. The powder was then ball-milled for 24 h in 160 ml of 2-propanol, with 560 g of 3Y-TZP spheres. The dried suspension was finally sieved under 125 μm, yielding powders characterized by an average particle size of 0.32 ± 0.03 μm and a specific surface area of $15\pm0.5\ m^2\ g^{-1}$.

The mixed powder named AZ5M was produced by mixing an appropriate amount of alumina and nanoscale unstabilized zirconia powder (UEP, DKKK, Japan, $d_{50}=200$ nm, $S_{BET}=23.5\ m^2/g$, primary crystallite size 25 nm). 200 g of the powder blend were milled in an attrition mill with 600 g of 3Y-TZP balls for 4 h at 500 rpm in 300 ml of 2-propanol. The milled dispersion was oven dried at 90 °C for 4 h and screened through a 100 μm mesh. These powders were characterized by an average particle size of 0.23 ± 0.03 μm and a specific surface area of $16.5\pm0.5\ m^2\ g^{-1}$.

Hot pressing (KCE, Germany) was carried out in a rectangular ($42\times22\ mm^2$) graphite die clad with boron nitride suspension. Two plates of AZ5M were pressed. In the case of AZ5C just one plate was pressed, as a smaller amount of powder was available. After evacuation and placing of a pre-load of 2 MPa the die was heated at 50 °C/min to the final temperature. The hot-pressing temperatures were varied between 1350 °C and 1600 °C in 50 °C increments. The samples were pressed under an axial load of 60 MPa for 1 h. Cooling was carried out in the press in argon atmosphere with the heater shut off.

2.2. Physical and microstructural characterization

The as-sintered samples were submitted to density measurements using the Archimedes' method. The rule of mixture was used to calculate the theoretical density (TD), assuming values of 3.98, 6.05 and $5.68\ g/cm^3$ for α-Al_2O_3, tetragonal and monoclinic ZrO_2, respectively. The TD ranged from $4.065\ g/cm^3$ for a fully monoclinic zirconia to $4.0835\ g/cm^3$ for a fully tetragonal one. Thus, for each sintered sample the actual TD was determined by evaluating the monoclinic volume fraction by means of XRD analysis, as outlined below.

The microstructural characterization of the sintered bodies was carried out by SEM (Scanning Electron Microscopy FEI QUANTA INSPECT 200 LV) on polished and thermally etched surfaces as well as on untreated fractured ones. Polishing was performed down to 1 μm with a diamond paste, whereas thermal etching was carried out at 100 °C below the sintering temperature, for 6 min.

2.3. Mechanical characterization

The preparation of samples for the mechanical tests was performed following a standardized procedure. After removing the grout by grinding, the ZTA plates were lapped with a 15 μm diamond suspension and polished with a 15 μm, 6 μm and 1 μm diamond suspension on both sides (Struers Rotopol, Denmark). Each plate was cut into 7 bars of 4 mm width and 1.5 mm thickness. The sides were ground and edges were bevelled with a 40 μm diamond disk and polished to a 15 μm finish to remove cutting grooves and edge defects. The remaining parts were kept for hardness testing and XRD. The 3-pt bending strength (σ_{3pt}) of 10 bars of AZ5M and 5 bars of AZ5C was determined according to DIN EN 6872 with a 15 mm span and a crosshead speed of 1.5 mm/min (Hegewald & Peschke, Germany). The Vickers hardness (HV_{10}, Bareiss, Germany, 5 indents) and microhardness ($HV_{0.1}$, Fischer, Germany, 12 indents) were determined and the indentation modulus E_{IND} was calculated from the loading/unloading curve of the microindentation measurement. Fracture toughness was determined by two independent procedures: Indentation strength in bending (ISB) tests were performed

on 4 bars of AZ5M and 2 bars of AZ5C, pre-notched with a HV_{10} indent in the middle of the tensile side and the residual strength for calculation of K_{ISB} was immediately measured in the same 3-pt setup [16]. Direct indentation (IND) crack length measurements were carried out on the five HV_{10} indents each: the indentation toughness K_{IND} was calculated with the model of Anstis et al. [17].

2.4. Phase composition

The phase composition of the zirconia was determined for the polished surfaces and fracture faces in the 27–33° 2θ-range. The intensities of the monoclinic (−111) and (111) reflexes as well as the tetragonal (101) reflex were integrated and the volumetric content of the monoclinic phase was calculated with the calibration curve of Toraya et al. [18]. The height of the transformation zone was calculated using the model of Kosmac et al. [19].

2.5. Residual stress analysis

The residual stress at the particle interface was calculated according to Kingery et al. [20], the overall hydrostatic residual stress was calculated according to Gregori et al. [21]. Toughness contribution of crack deflection was calculated according to Taya et al. [22]. The influence of microcracking was evaluated using the formalism of Tsukuma et al. [23]. The contribution of transformation toughening was calculated according to McMeeking and Evans [24].

3. Results

3.1. Physical and microstructural characterization

Fig. 1 shows the evolution of density with hot-pressing temperature for the two sets of composites AZ5C and AZ5M.

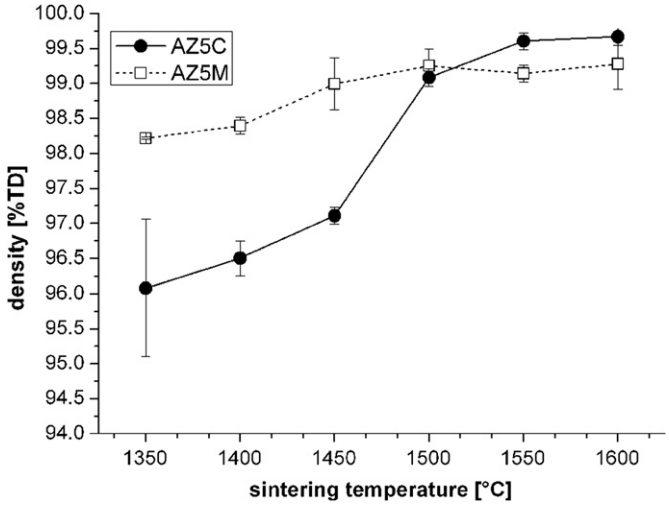

Fig. 1. Density (%TD) vs. sintering temperature of AZ5 samples.

The significantly lower sinterability of the coated powder compared to the mixed compound was evident. In fact, AZ5M reached a density >98% TD at the lowest sintering temperature, while AZ5C needed 1500 °C to reach the same density level. However, at the higher hot-pressing temperatures (1500 °C–1600 °C) both composites reached very high densities, with slightly higher maximum values for AZ5C. The different sintering behavior of AZ5C and AZ5M at the lower hot-pressing temperature can be partially addressed to differences in starting particle size, being AZ5M slightly finer than AZ5C. A possible further explanation can be found in the lower crystallization degree of zirconia in the coated powders. In fact, in AZ5C consolidation with concurrent crystallization occurred during hot-pressing, thus requiring higher maximum temperature for reaching full density.

SEM observation allowed us to demonstrate significant microstructural differences between the two sets of materials, due to the elaboration route of the composite powders. In fact, in AZ5C the zirconia particles dispersion inside the alumina matrix was not completely homogeneous and zirconia agglomerates were sometimes observed (see Fig. 2a). Such a drawback has been already partially observed in the past [25] when yttria-coated powders were consolidated under non-conventional sintering routes. Once again, it was imputed to the low crystallization degree of the second-phase precursor which produced ultrafine and well distributed particles when pressure-less sintered, but less homogenous microstructures under hot-pressing or, even more, spark plasma sintering conditions. On the contrary, this drawback was completely absent in AZ5M materials, which presented very homogeneous microstructures. This result highlights that, if correctly processed, (nano)composites ceramics with high density and controlled microstructures can be successfully produced from the mixing and milling route [13,14]. Fig. 2(a–f) shows the microstructure (images of polished and thermally etched surfaces) of some of the sintered materials. Precisely, they refer to AZ5M and AZ5C sintered at the lowest (1350 °C), at an intermediate (1500 °C) and at the higher (1600 °C) hot-pressing temperature.

AZ5C hot-pressed at 1350 °C still contained some residual porosity, according to its low final density. On the opposite, the respective material by mechanical mixing as well as all other samples showed in the images are highly dense. At the lower hot-pressing temperatures, inter-type AZ5C and AZ5M composites were observed, whereas by increasing the sintering temperature, the microstructure shifted from inter-type to an intra-inter structure (though with a predominance of inter-type zirconia grains). Clearly, the amount of zirconia was not able to block all 4 junctions and prevent alumina grain growth [26]. By comparing AZ5C and AZ5M at the same hot-pressing temperatures, AZ5C always showed larger grain sizes for both matrix and dispersion, as evidenced in Fig. 3. In the case of AZ5C, the initial grain sizes at 1350 °C were about 300 nm for zirconia and 700 nm for alumina. At 1600 °C they grew up to 650 nm and 2.7 μm, respectively.

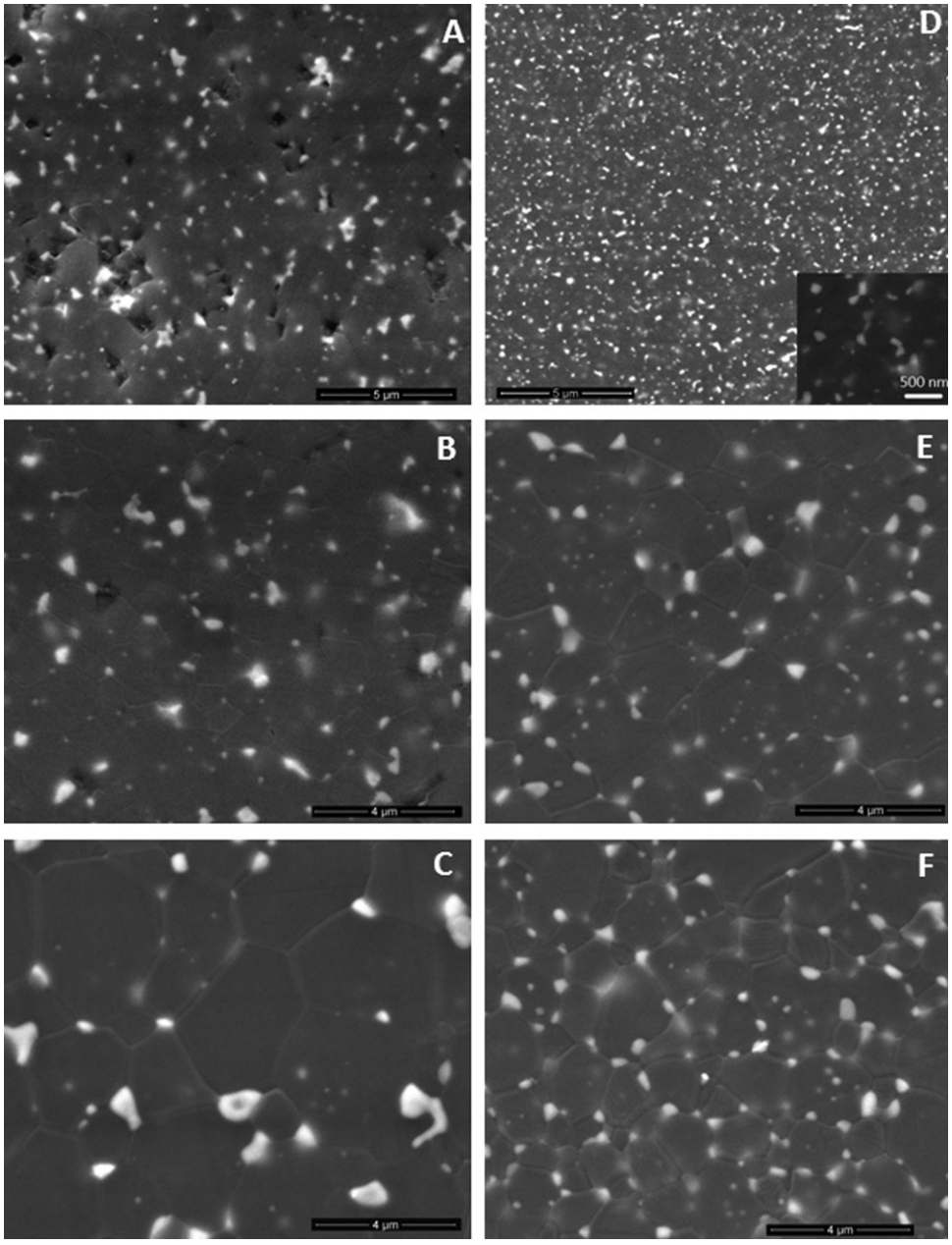

Fig. 2. SEM images of AZ5C (A–C) and AZ5M (D–F) sintered at 1350 °C (A,D), 1500 °C (B,E) and 1600 °C (C,F).

The growth process seemed not to proceed continuously but step-wise with an increase every 100 °C in hot-pressing temperature. In the case of AZ5M, the initial grain sizes at 1350 °C were finer, with 200 nm for zirconia and 350–400 nm for alumina. This zirconia grain size was thus identical to the size of zirconia agglomerates in the starting powder. Grain growth in the mixed compound proceeded more continuously, but with a considerable lower extent. In fact, the final values were about 400 nm for zirconia and 1.6 μm for alumina. In addition, it can be observed a higher standard deviation of alumina average grain size in AZ5C compared to AZ5M (especially at the higher hot-pressing temperatures). This was justified by the less homogeneous distribution of zirconia particles in the former materials, which exerted a less controlled and effective pinning on the alumina grain boundaries.

The fracture surfaces showed an inter-granular fracture mode in both AZ5C and AZ5M sintered at the lower temperatures (up to 1400 °C). Trans-granular fracture paths were increasingly observed by increasing the sintering temperature and thus the matrix grain size.

3.2. Mechanical characterization

In Fig. 4 the Vickers hardness HV_{10} is shown. AZ5C hot-pressed at 1350 °C showed a very low hardness, as expected on the ground of its low density. HV_{10} significantly increased at 1400 °C, due to the slightly higher

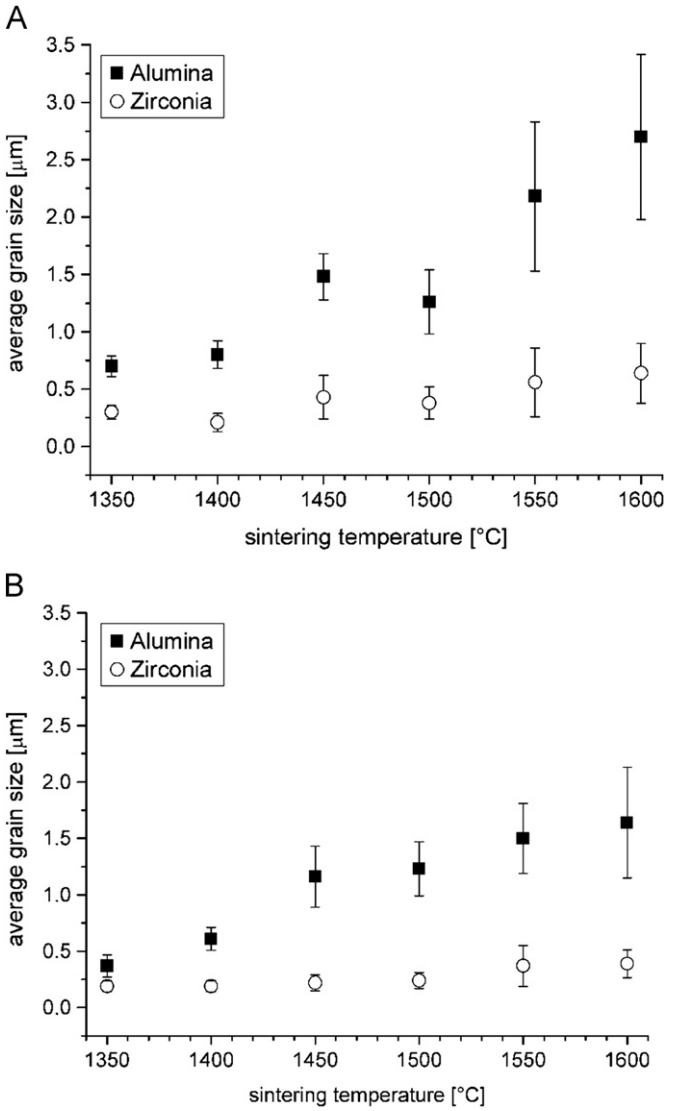

Fig. 3. Average alumina and zirconia grain size vs. sintering temperature of (A) AZ5C and (B) AZ5M.

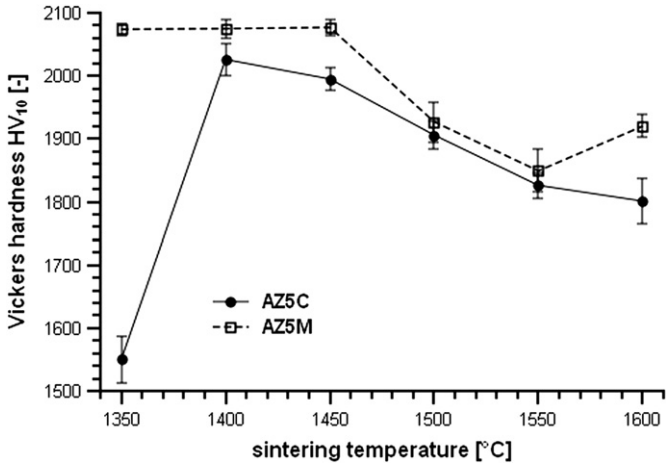

Fig. 4. Vickers hardness HV_{10} vs. sintering temperature of AZ5 samples.

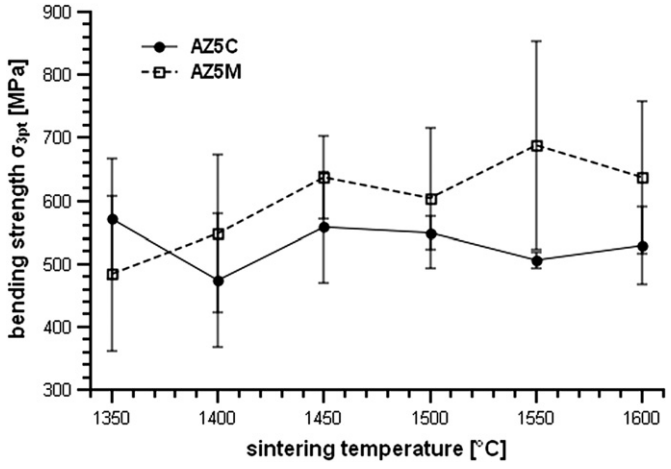

Fig. 5. Bending strength vs. sintering temperature of AZ5 samples.

density and fine microstructure of the material. On the opposite, AZ5M materials were characterized by high hardness, even at the lower hot-pressing temperature, according to their high final density and ultra-fine microstructure. Above 1400 °C (AZ5C) and 1450 °C (AZ5M) the hardness started to decline almost linearly from >20 GPa to 18 GPa (at 1600 °C), due to the grain size increase with the temperature.

Microhardness $HV_{0.1}$ (not shown) was more sensitive to grain size, but similarly to the hardness HV_{10}, it showed a declining trend starting from 1400 °C (AZ5M)–1450 °C (AZ5C).

The indentation modulus (not shown) of AZ5C and AZ5M ranged between 380 GPa and 410 GPa, except for AZ5C hot-pressed at 1350 °C, which showed a lower value of 325 GPa. Once again, this was due to the low sintered density of the material.

Fig. 5 shows the bending strength of the two sets of composites vs. hot-pressing temperature. Also in this case, both final density and grains size could affect the evolution of strength with the sintering temperature. The trend was quite flat for AZ5C, while it slightly increased with the temperature, reaching a maximum value of 680 MPa at 1550 °C, for AZ5M. This latter material, which benefited of finer grain size and higher microstructural homogeneity, presented average strength 100–150 MPa higher than AZ5C.

The fracture toughness determined by ISB method is displayed in Fig. 6. For both materials toughness rose with hot-pressing temperature. In the case of AZ5M toughness rose from 3.5 MPa $\times\sqrt{m}$ at 1350 °C to 4.5 MPa $\times\sqrt{m}$ at 1600 °C. The toughness of AZ5C was in average $\sim$0.2 MPa $\times\sqrt{m}$ higher than that of AZ5M.

The indentation toughness measured according to Anstis et al. [17] (not shown) presented a similar trend as ISB toughness but lower absolute values and a slightly stronger discrimination between AZ5C and AZ5M. In fact, the toughness of AZ5C was in average 0.3–0.4 MPa $\times\sqrt{m}$ higher than in AZ5M. Toughness exceeded the toughness of plain fine-grained alumina, which reaches 2.75–3.5 MPa $\times\sqrt{m}$ depending on grain size and measuring protocol.

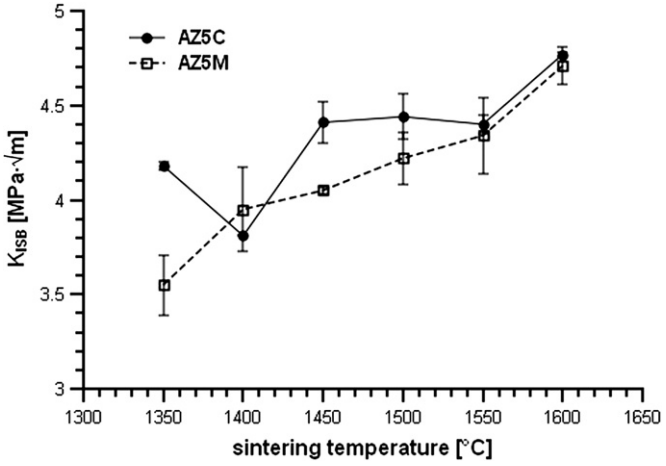

Fig. 6. ISB toughness vs. sintering temperature of AZ5 samples.

3.3. Phase composition

The monoclinic zirconia volume fraction in AZ5C and AZ5M is shown in Fig. 7(a) and (b), respectively.

In both materials, a rising trend in monoclinic content in polished surfaces with increasing temperature (and thus increasing zirconia grain size) can be observed. The monoclinic content in AZ5M was generally much lower than in AZ5C. In fact, in the former material it ranged from about 0.04–0.22, whereas in the second one from about 0.20–0.55. The monoclinic content in fracture faces rose as well. The transformability, which is defined as the difference in monoclinic percentage in fractured and polished samples, was higher for the AZ5C samples (ranging between 15 and 35%) than for AZ5M ones (from 2 to 20%). At the first glance it was thus surprising to find very similar toughness for both materials as transformability in AZ5C was almost the double than in AZ5M, as transformation toughening was considered the dominant toughening mechanism in fine-grained ZTA.

A more detailed analysis of the XRD data of the fracture faces (Fig. 8) showed that besides the expected reflexes $(-111)_m$ at 28.3°, $(101)_t$ at 30.2× and $(111)_m$ at 31.6×, one or two additional reflexes at 29–29.3× can be identified in the range between the $(-111)_m$ and $(101)_t$ reflex. In the polished surfaces these reflexes were absent. These additional reflexes have been previously detected in fracture faces of other ZTA and TZP materials, and they may hint at a contribution by ferroelastic toughening [27,28]. It can be also observed that the $(101)_t$ reflex in the two materials was shifted in different directions: while in AZ5M the location of the $(101)_t$ reflex migrated from higher to lower 2θ-values, the opposite tendency was observed for AZ5C. This indicates a different residual stress situation.

3.4. Residual stress and contributions from different reinforcing mechanisms

Assuming that a composite material of alumina with a coefficient of thermal expansion (CTE) of $\sim 8 \times 10^{-6}\,K^{-1}$ (α_A) and a tetragonal zirconia dispersion with a CTE of $11 \times 10^{-6}\,K^{-1}$ (α_z) is stress free at the sintering temperature, residual stresses will arise during cooling to room temperature. As the zirconia dispersion, consisting of isolated particles, shrinks more than alumina, the matrix will be left under compressive stress and the dispersion under tensile. Tetragonal zirconia exceeding a critical grain size can thus transform to monoclinic during cooling. In such a way, the composite can reduce its level of stress by transformation. Above a certain monoclinic content which, according to Gregori et al. [21], is reached at ~25 vol% the situation reverses and the matrix comes under tensile stress. The tendency of zirconia to transform depends on grain size, morphology and location. By applying the formalism of Gregori et al. [21], the residual stress situation in alumina $\langle \sigma \rangle_A$ can be calculated according to the following equation:

$$\langle \sigma \rangle_A = K^*(\varepsilon_{ETM} + X_m \varepsilon^T) \quad (1)$$

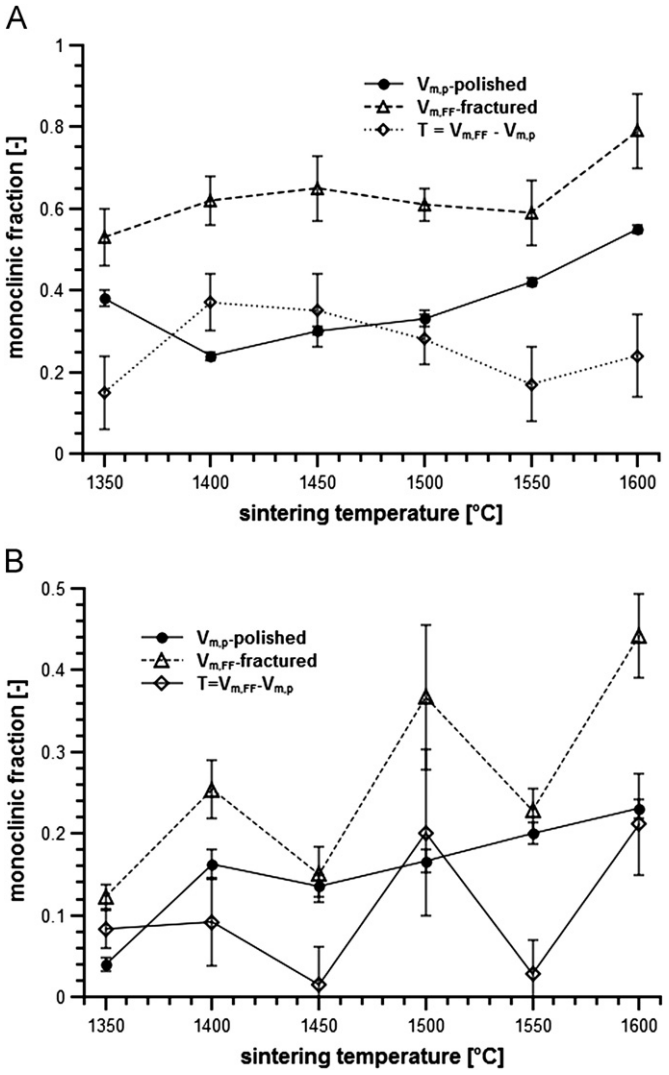

Fig. 7. Monoclinic fraction in polished surface and fracture face vs. sintering temperature of AZ5C (A) and AZ5M (B) samples.

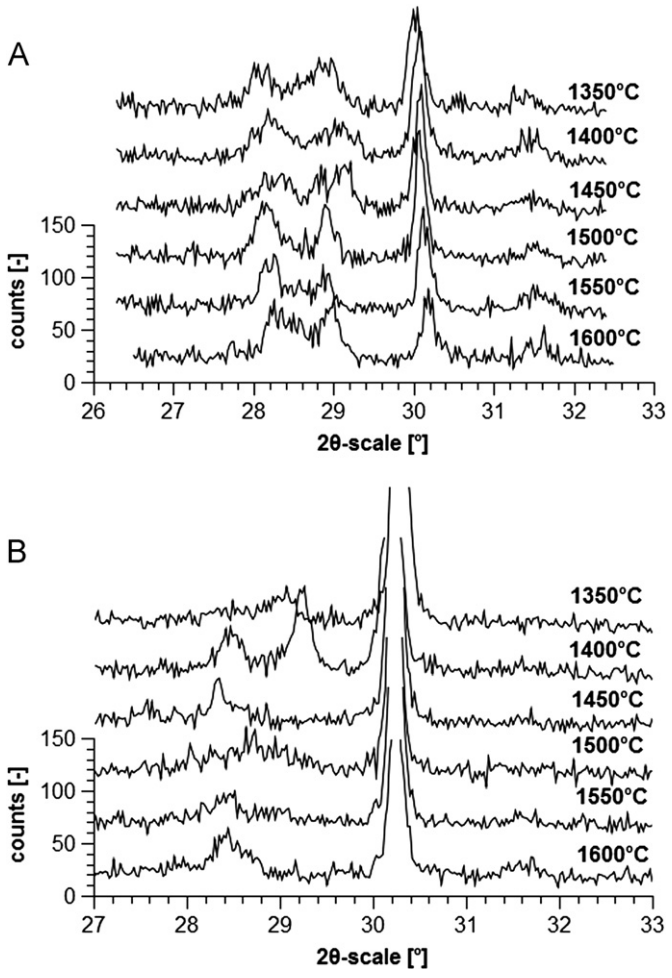

Fig. 8. XRD of the fracture face of AZ5C (A) and AZ5M (B) in the 26.5–32.5° 2θ-range.

where ε^T is the transformation strain, X_m is the monoclinic volume fraction, ε_{ETM} is the elastic thermal mismatch strain given by

$$\varepsilon_{ETM} = (\alpha_z - \alpha_A)(T_z - T_{sfz})$$

In which T_0 is room temperature and T_{sf} is the temperature below which the elastic stress is frozen-in, here assumed as the sintering temperature.

K^* is given by

$$K^* = \frac{3nK_A}{K_z f_A + nK_A f_A + nK_Z f_Z + K_z f_z}$$

In which K is the bulk modulus, f is the constituents volume fraction, n is given by

$$n = \frac{2(1-2v_A)}{1+v_A}$$

where v_A is the Poisson modulus of alumina (subscripts A and Z refer to alumina and zirconia, respectively). For a sake of clarity, the physical constant used for calculating the residual stress are collected in Table 1.

For alumina 5 vol% zirconia composites, containing a purely tetragonal dispersion ($X_m=0$), we can calculate a compressive hydrostatic stress of 49–58 MPa (depending on the sintering temperature) in the matrix and a tensile stress of 940–1110 MPa for the dispersion, according to the following static equilibrium condition

Table 1
Physical constant used for calculating the residual stress.

	Alumina	Zirconia
CTE (α)	$\sim 8\times10^{-6}$ °C^{-1}	$\sim 11\times10^{-6}$ °C^{-1}
Bulk modulus (K) (GPa)	250	150
Poisson's ratio (v)	0.27	
Cooling rate ($T_0 - T_{sf}$)	1325–1575 °C	
ε^T	0.016	

$$f_A \langle \sigma \rangle_A + f_Z \langle \sigma \rangle_Z = 0 \quad (2)$$

Such compressive stress in alumina decreased with increasing the monoclinic zirconia content, reached the neutral state at 25–29% of transformation and converted to a tensile stress for higher monoclinic zirconia concentration.

By using Eq. (1), we calculated the evolution of the hydrostatic stress in the alumina matrix with the sintering temperature. Data of AZ5M and AZ5C phase composition were taken from Fig. 7. As the total stress in the composite is zero (Eq. (2)), the corresponding hydrostatic stress in the zirconia dispersion can be also easily calculated. Results showed that the alumina matrix was under compressive stress in AZ5M samples, and under tensile stress in AZ5C ones, due to the high monoclinic content in these materials.

For intercrystalline zirconia particles, relaxation effects such as grain boundary sliding during cooling will reduce the stress. However, for zirconia particles inside the matrix, no stress reduction can be expected. According to Taya et al. [22] (Eq. (3)), who investigated the crack deflection by residual cooling stress generated by TiB_2 dispersion in a SiC matrix, the stress intensity factor can be calculated according to the following Eq. (3)

$$\Delta K_I{}^{CD} = 2q\sqrt{\frac{2(\lambda - d)}{\pi}} \quad (3)$$

With a residual stress q (see Fig. 9), a mean particle diameter d (see Fig. 3), a mean interparticle distance $\lambda = 1.085d/\sqrt{f_p}$, where f_p is the particle fraction (0.05), ΔK_I^{CD}, i.e. the increase of the stress intensity factor at the crack tip, can be calculated. Results of calculation showed that the toughening effect was positive for the AZ5M materials and negative for most of the AZ5C ones, but negligible in all cases. In fact, ΔK_I^{CD} ranged from -0.07 to $+0.03$ MPa $\times \sqrt{m}$. The effect of residual stress on the strength may be more important as we may assume that the stress state of the matrix will add to the operating stress. From Fig. 9, the differences in residual stress between AZ5C and AZ5M were 20–70 MPa. This effect may explain at least partly the higher strength of the AZ5M composite.

Microcracking according to Tsukuma et al. [23] is possible if the size of the dispersion exceeds a critical

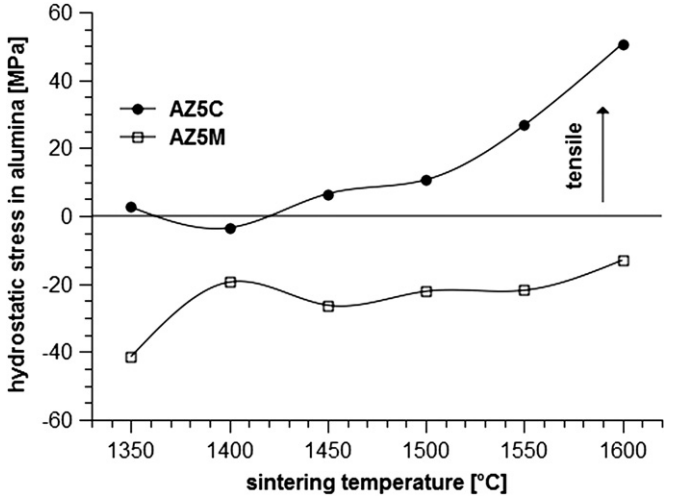

Fig. 9. Residual average hydrostatic stress in the alumina matrix of AZ5 composites.

particle size D_s, which can be calculated with Eq. 4

$$D_s = \frac{10\gamma_m}{(\Delta\varepsilon)^2 E} = 1.1\text{–}1.6\ \mu m \tag{4}$$

where γ_m is the fracture energy for microcracking ($\sim$1 J/m^2), E the elastic modulus of the composite ($\sim$400 GPa, as experimentally determined) and $\Delta\varepsilon = \Delta\alpha\Delta T$ the product of CTE and temperature difference (see values in Table 1). The calculated values were higher than the measured zirconia particle sizes. So, a contribution of microcracking by tetragonal particles was not expected. In the case of transformed zirconia particles, the total strain is dominated by the transformation strain ε^T (0.016) which is four times larger than the thermal strain $\Delta\varepsilon$ (0.004). So, D_s decreases to 0.1 μm. Thus, even small monoclinic zirconia particles could cause microcrack toughening. However we can expect that all particles $< \sim$0.4 μm will maintain their tetragonal structure during cooling. As a consequence, microcracking can only deliver a significant toughness increment in case of materials with a mean zirconia particle size exceeding this value (AZ5C hot-pressed at 1550 or 1600 °C).

According to McMeeking and Evans [24], contribution of transformation toughening K_I^T can be described by the following equation:

$$K_I{}^T = XEe_T V_f \sqrt{h} \tag{5}$$

where X is a constant which depends on the transformation behavior and may vary between 0.22 for pure dilatation to 0.55 for dilatation and strain (the present calculation was carried out using a factor of 0.27 as for Y-TZP as reported by Swain [29]); E is the elastic modulus; e_T the volumetric transformation strain (0.05); V_f the fraction of transformed zirconia (Fig. 7) multiplied with the zirconia content (5 vol%); h the half height of the transformation zone.

The value of h (Eq. 5) can be determined according to Kosmac et al. [19] from the phase composition of fractured faces (X_{fract}) and polished surface (X_{Bulk}) with the maximum transformability (X_{trans} = 1) and the X-ray penetration depth μ (0.007 mm for alumina 5 vol% zirconia)

$$h = \frac{\sin(15^\circ)}{2\mu} \ln\left(\frac{X_{Bulk} - X_{trans}}{X_{fract} - X_{trans}}\right) \tag{6}$$

As a result, h varied between 5 and 14 μm for AZ5C and between 0.2 and 6 μm for AZ5M, whereas toughness increment of 0.1–0.45 MPa $\times \sqrt{m}$ and 0.01–0.2 MPa $\times \sqrt{m}$ were respectively calculated for AZ5C and AZ5M.

4. Discussion

AZ5 composites derived from coated and mixed powders present quite similar mechanical properties. The main differences were slightly higher toughness and lower strength for the AZ5C material. An analysis of microstructure and phase composition and a calculation of the state of residual stress have revealed that these two apparently similar materials have completely different features in detail. In the case of AZ5M, the finer grain size of zirconia resulted in a lower transformability; the alumina matrix was under compressive stress and the dispersion under tensile; transformation zones were significantly smaller and thus the transformation toughness increment was very moderate.

A completely different situation was determined in AZ5C. These materials had in average larger zirconia grains with a fraction beyond the critical size, which resulted in high monoclinic content. This induced an opposite stress situation, larger transformation zone size and transformation toughness increment. In AZ5C samples sintered at 1550–1600 °C, whose monoclinic zirconia grains exceed a critical size, we expected some toughness contribution by microcracking.

Adding up the calculated toughness increments and assuming an optimistic threshold toughness K_0 of $\sim$3.5 MPa $\times \sqrt{m}$, we obtained a total toughness of $\sim$3.6–3.7 MPa $\times \sqrt{m}$ for AZ5M and $\sim$3.6–4 MPa $\times \sqrt{m}$ for AZ5C which was lower than the measured values. An increment of $\sim$0.5 MPa $\times \sqrt{m}$ remained which was not explained yet. One unknown variable was the value X in Eq. (5). A higher value would linearly increase the transformation toughness increment. However, such a high value was unlikely due to the constraint of the rigid alumina matrix.

A contribution of ferroelastic toughening was suspected from the XRD analysis. Ferroelastic toughening results in shear but no dilatation as thus should deliver about the same toughness increment as a weak phase transformation. Moreover as the ferroelastic transformation is not accompanied by volume expansion it will not be restrained by the high rigidity of the matrix. As a ferroelastic transformation according to Virkar requires a high stress of $\sim$1.65 GPa this seems unlikely at first sight as the strength of the composites is $<$ 700 MPa [30]. In the composite there was however a superimposed residual stress field which can add to operating stress. According to Kingery et al. [20], directly at the interface of tetragonal zirconia and alumina

there was a residual hoop stress of 1100–1300 MPa, similar to the residual hydrostatic stress on zirconia determined from the Gregori et al. model (940–1110 MPa) of [20,21] (depending on sintering temperature). This residual stress added to 700 MPa bending stress so that the total stress came close to 2 GPa. Ferroelastic toughening could thus provide the missing $\sim 0.5\ \text{MPa} \times \sqrt{m}$ in case of AZ5M. In case of AZ5C only the fine-grained fraction of zirconia will be affected so that we may expect—if any—a considerably lower contribution by ferroelastic toughening.

5. Conclusion

Two types of 5 vol% zirconia reinforced alumina composites were manufactured from the same alumina powder, and consolidated under identical hot-pressing conditions. Microstructure, mechanical properties and phase compositions were investigated and the residual stress situations in composites sintered under different conditions were calculated. The composite AZ5C derived from zirconia coated alumina showed a less homogeneous and fine microstructure, higher toughness and transformability, but at a slightly reduced level of hardness and strength. The matrix in this composite was under tensile stress, the transformability of zirconia was high and the transformation zones were very high. The composite AZ5M produced by conventional mixing and milling technique using a unstabilized nanoscale zirconia as reinforcement had a finer alumina and zirconia grain size, higher strength and hardness, lower toughness and transformability and transformation zone sizes were considerably smaller. The powder manufacturing process demonstrated to strongly affect the features of alumina-zirconia nanocomposites. Coming investigations will focus on making composite materials with higher zirconia content and potentially higher strength and toughness. The scale up of the powder preparation process will be a key issue in transferring the results to technical applications by using shaping technologies like casting, cold pressing and injection molding, followed by pressure-less sintering.

References

[1] J. Wang, R. Stevens, Review zirconia-toughened alumina (ZTA) ceramics, Journal of Materials Science 34 (1989) 3421–3440.

[2] G. Pezzotti, T. Saito, Y. Takahashi, K. Fukatsu, N. Sugano, Surface topology of advanced alumina/zirconia composite femoral head as compared with commercial femoral heads made of monolithic zirconia, Journal of the American Ceramic Society 94 (2010) 945–950.

[3] M. Rühle, N. Claussen, A. Heuer, Transformation and microcrack toughening as complementary processes in ZrO_2-toughened Al_2O_3, Journal of the American Ceramic Society 69 (1986) 195–197.

[4] N. Claussen, Fracture toughness of Al_2O_3 with an unstabilized ZrO_2 dispersed phase, Journal of the American Ceramic Society 59 (1976) 49–51.

[5] P. Becher, M. Swain, Grain-size-dependent transformation behavior in polycrystalline tetragonal zirconia, Journal of the American Ceramic Society 75 (1992) 493–502.

[6] A.H. Heuer, N. Claussen, W.M. Kriven, M. Rühle, Stability of tetragonal ZrO_2 particles in ceramic matrices, Journal of the American Ceramic Society 65 (1982) 642–650.

[7] K. Biotteau-Deheuvels, L. Zych, L. Gremillard, J. Chevalier, Effects of Ca-, Mg- and Si-doping on microstructures of alumina–zirconia composites, Journal of the European Ceramic Society http://dx.doi.org/10.1016/j.jeurceramsoc.2011.11.011, 2011.

[8] G.L. Messing, M. Kumagai, Low-temperature sintering of seeded sol–gel-derived, ZrO_2,-toughened Al_2O_3 composites, Journal of the American Ceramic Society 12 (1989) 40–44.

[9] A. DeAza, J. Chevalier, G. Fantozzi, M. Schehl, R. Torrecillas, Slow-crack-growth behavior of zirconia-toughened alumina ceramics processed by different methods, Journal of the American Ceramic Society 86 (2003) 115–120.

[10] P. Palmero, V. Naglieri, J. Chevalier, G. Fantozzi, L. Montanaro, Alumina-based nanocomposites obtained by doping with inorganic salt solutions: application to immiscible and reactive systems, Journal of the European Ceramic Society 29 (2009) 59–66.

[11] P. Palmero, C. Esnouf, Phase and microstructural evolution of yttrium-doped nanocrystalline alumina: a contribution of advanced microscopy techniques, Journal of the European Ceramic Society 31 (2011) 507–516.

[12] P. Palmero, F. Kern, M. Lombardi, R. Gadow, Role of immiscible and miscible second phases on the sintering kinetics and microstructural development of nano-crystalline α-Al_2O_3-based materials, Ceramics International 37 (2011) 3547–3556.

[13] F. Kern, Sintering conditions, microstructure and properties of alumina 10 vol% zirconia nanocomposites, Journal of Ceramic Science and Technology 3 (2012) 1–8.

[14] F. Kern, Microstructure and mechanical properties of hot-pressed alumina—5 vol% zirconia nanocomposites, Journal of Ceramic Science and Technology 1 (2010) 69–74.

[15] P. Palmero, A. Sola, V. Naglieri, D. Bellucci, M. Lombardi, V. Cannillo, Elaboration and mechanical characterization of multiphase alumina-based ultra-fine composites, Journal of Materials Science 47 (2012) 1077–1084.

[16] P. Chantikul, G.R. Anstis, B.R. Lawn, D.B.A. Marshall, A critical evaluation of indentation techniques for measuring fracture toughness. II. Strength method, Journal of the American Ceramic Society 64 (1981) 539–543.

[17] G.R. Anstis, P. Chantikul, B.R. Lawn, D.B.A. Marshall, A critical evaluation of indentation techniques for measuring fracture toughness. I. Direct crack measurements, Journal of the American Ceramic Society 64 (1981) 533–538.

[18] H. Toraya, M. Yoshimura, S. Somiya, Calibration curve for quantitative analysis of the monoclinic-tetragonal ZrO_2 system by X-ray diffraction, Journal of the American Ceramic Society 67 (1984) C119–C121.

[19] T. Kosmac, R. Wagner, N. Claussen, X-ray determination of transformation depths in ceramics containing tetragonal ZrO_2, Journal of the American Ceramic Society 64 (1981) C72–C73.

[20] W.D. Kingery, H.K. Bowen, D.R. Uhlmann, Introduction to Ceramics, Wiley, New York, 1976, pp. 785.

[21] G. Gregori, W. Burger, V. Sergo, Piezo-spectroscopic analysis of the residual stresses in zirconia-toughened alumina ceramics: the influence of the tetragonal-to-monoclinic transformation, Materials Science and Engineering A271 (1999) 401–406.

[22] M. Taya, S. Hayashi, A.S. Kobayashi, H.S. Yoon, Toughening of a particulate-reinforced ceramic-matrix composite by thermal residual stress, Journal of the American Ceramic Society 73 (1990) 1382–1391.

[23] K. Tsukuma, K. Ueda, M. Shimada, Strength and fracture toughness of isostatically hot-pressed composites of Al_2O_3 and Y_2O_3-partially stabilized ZrO_2, Journal of the American Ceramic Society 68 (1985) C4–C5.

[24] R. McMeeking, A.G. Evans, Mechanics of transformation-toughening in brittle materials, Journal of the American Ceramic Society 65 (1982) 242–246.

[25] P. Palmero, G. Fantozzi, F. Lomello, G. Bonnefont, L. Montanaro, Creep behaviour of alumina/YAG composites prepared by different sintering routes, Ceramics International 38 (2012) 433–441.

[26] F.F. Lange, M. Hirlinger, Hindrance of grain growth in Al_2O_3 by ZrO_2 inclusions, Journal of the American Ceramic Society 67 (1984) 164–168.
[27] F. Kern, M. El Ezz, R. Gadow, Thermoplastic ceramic injection molding of zirconia toughened alumina components, in: T. Ohji, M. Singh, S. Mathur (Eds.), Advanced Processing and Manufacturing Technologies for Structural and Multifunctional Materials IV, John Wiley &Sons, Hoboken, http://dx.doi.org/10.1002/9780470944066.ch21 Vol. 31, 2010.
[28] F. Kern, R. Gadow, Ytterbia (2.25 mol%) stabilised zirconia (Yb-TZP) manufactured from coated nanopowder, Advances in Applied Ceramics http://dx.doi.org/10.1179/1743676111Y.0000000071, 2012.
[29] M.V. Swain, L.R.F. Rose, Strength limitations in transformation-toughened zirconia alloys, Journal of the American Ceramic Society 69 (1986) 511–518.
[30] A.V. Virkar, D.L. Johnson, Fracture behavior of ZrO_2–Zr composites, Journal of the American Ceramic Society 60 (1977) 514–519.